Copper(I) and silver(I) chemistry of vinyltrifluoroborate supported by a bis(pyrazolyl)methane

Adway O. Zacharias, James Mao,* Kwangho Nam, H. V. Rasika Dias*

Department of Chemistry and Biochemistry, The University of Texas at Arlington, Arlington, Texas 76019, USA

AUTHOR INFORMATION

Corresponding Authors

H. V. Rasika Dias, *E-mail: dias@uta.edu;* ORCID: 0000-0002-2362-1331

James Mao, *E-mail: xiaojian@uta.edu*

Key words:

Alkene chemistry, Organotrifluoroborate, Silver, Copper, Density functional calculations

Abstract: Although unsaturated organotrifluoroborates are common synthons in metal-organic chemistry, their transition metal complexes have received scant attention. The $[CH_2(3,5\text{-}(CH_3)_2Pz)_2]Cu(CH_2{=}CHBF_3)$, $(SIPr)Cu(MeCN)(CH_2{=}CHBF_3)$ and $[CH_2(3,5\text{-}(CH_3)_2Pz)_2]Ag(CH_2{=}CHBF_3)$ represent rare, isolable molecules featuring a vinyltrifluoroborate ligand on coinage metals. X-ray crystal structures show the presence of three coordinate metal sites in these complexes. The vinyltrifluoroborate group binds asymmetrically to the metal site in $[CH_2(3,5\text{-}(CH_3)_2Pz)_2]M(CH_2{=}CHBF_3)$ (M = Cu, Ag) with relatively closer M-$C(H)_2$ distances. Computed structures of $[CH_2(3,5\text{-}(CH_3)_2Pz)_2]M(CH_2{=}CHBF_3)$ and $M(CH_2{=}CHBF_3)$ however, have shorter M-$C(H)BF_3$ than M-$C(H)_2$ distances. These molecules feature various inter- or intra-molecular contacts involving fluorine of the BF_3 group, possibly affecting these M-C distances. The binding energies of $[CH_2{=}CHBF_3]^-$ to Cu^+, Ag^+ and Au^+ have been calculated at the wB97XD/def2-TZVP level of theory, in the presence and absence of the supporting ligand $CH_2(3,5\text{-}(CH_3)_2Pz)_2$. The calculation shows that Au^+ has strongest binding to the $[CH_2{=}CHBF_3]^-$ ligand, followed by Cu^+ and then Ag^+, irrespective of the presence of the supporting ligand. However, in all three metals, the supporting ligand weakens the binding of olefin to the metal. The same trends are also discovered from the analysis of the σ-donation and π-backbonding interactions between the metal fragment and the π and π* orbitals of $[CH_2{=}CHBF_3]^-$.

Introduction

Organotrifluoroborates such as alkenyl-, alkynyl- and aryl-trifluoroborates are useful reagents in organic chemistry.[1] They are employed most frequently in the metal catalyzed, Suzuki-Miyaura cross-coupling reactions leading to new C-C bonds. Other metals including copper also mediate important chemical processes involving organotrifluoroborates.[1a, 1d, 2] Interestingly, despite the wide utility of unsaturated trifluoroborates as organic synthons in metal-organic chemistry, their π-donor ligand potential towards transition metal ions has received relatively less attention. For example, a search of Cambridge Structural Database[3] reveals that structurally authenticated d-block complexes involving π-bonded organotrifluoroborate ligands are limited to several ferrocenyltrifluoroborates (i.e., iron complexes of cyclopentadienyl-trifluoroborates, e.g., **1**, Figure 1),[4] a phenyltrifluoroborate adduct of ruthenium, **2**,[5] and (SIPr)Ag(CH_2=$CHBF_3$) (**3**) and (IPr*)Ag(CH_2=$CHBF_3$) (SIPr = 1,3-bis(2,6-diisopropylphenyl)imidazolin-2-ylidene; IPr* = 1,3-bis(2,6-bis(diphenylmethyl)-4-methylphenyl)imidazol-2-ylidene) featuring a vinyltrifluoroborate ligand on silver(I) supported by *N*-heterocyclic carbenes (NHCs).[6]

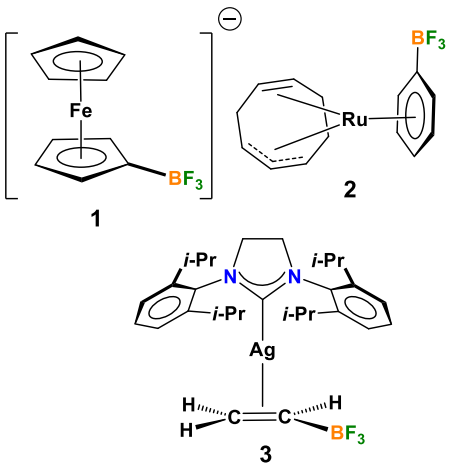

Figure 1. Organotrifluoroborate complexes of transition metal ions

As a part of our ongoing activities involving metal-olefin complexes,[7] we became interested in the coordination chemistry of vinyltrifluoroborate ion ($[CH_2=CHBF_3]^-$)[8] since it represents a virtually unexplored, formally negatively charged, π-donor ligand for metal ions. In addition, asymmetrically substituted olefins such as $[CH_2=CHBF_3]^-$ could provide isolable molecules that feature pseudo η^1-coordination mode, which is of interest as a model for olefin activation step towards nucleophiles.[9]

Recently we reported the isolation of silver complexes (SIPr)Ag($CH_2=CHBF_3$) (**3**) and (IPr*)Ag($CH_2=CHBF_3$) of this interesting ligand.[6] Furthermore, calculated metal-ligand binding energies show that $[CH_2=CHBF_3]^-$ is a significantly better ligand for Ag(I) than $CH_2=CH_2$ or isoelectronic $CH_2=CHCF_3$. Here we describe an expansion of that effort to uncover the copper complexes, a comparison of copper and silver chemistry, and a detailed computational study of vinyltrifluoroborates of Cu, Ag and Au. We note that coinage metal complexes involving organoborates are also of interest as reaction intermediates and for PET imaging work.[10] In addition, reactions involving vinylcuprates with BF_3 additives[11] as well as copper catalyzed reactions of vinyltrifluoroborates are known,[12] in which the formation of copper vinyltrifluoroborates as intermediates is a possibility. To test this hypothesis, we have also probed the utility of pre-formed copper-vinyltrifluoroborate as a catalyst for the synthesis of functionalized 1,2-disubstituted cyclopropyltrifluoroborates, and as a stoichiometric reagent to facilitate ring opening reactions of an unhindered epoxide.

Results and discussion:

The NHC supported (SIPr)Cu(MeCN)(CH_2=$CHBF_3$) (**4**) was synthesized by treating (SIPr)$CuNO_3$ with K(CH_2=$CHBF_3$) in dichloromethane/acetonitrile and isolated as a white, fairly air stable solid in 90% yield (Scheme 1). It shows good solubility in halogenated solvents like CH_2Cl_2 and $CHCl_3$ but is insoluble in hexane or Et_2O and has been characterized by multinuclear NMR spectroscopy and X-ray crystallography. The $^{13}C\{^1H\}$ NMR signal of the copper bound $\underline{C}H_2$=$CHBF_3$ could be observed as a singlet at δ 99.9 ppm for (SIPr)Cu(MeCN)(CH_2=$CHBF_3$). It can be compared to the corresponding resonance in (SIPr)Ag(CH_2=$CHBF_3$) (that has an η^2-bound [CH_2=$CHBF_3$]$^-$ moiety), [(IPr)$_2$Ag][CH_2=$CHBF_3$] (that has a free [CH_2=$CHBF_3$]$^-$ moiety)[6] and K(CH_2=$CHBF_3$)[13] which is observed at δ 114.3, 120.1 and 121.6 ppm, respectively. Thus, the copper(I) coordination has a more significant effect on [CH_2=$CHBF_3$]$^-$ group.

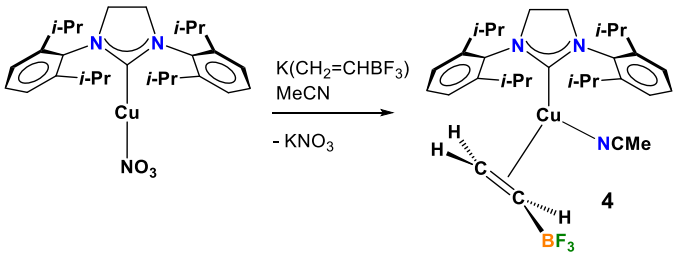

Scheme 1. Synthesis of (SIPr)Cu(MeCN)(CH_2=$CHBF_3$)

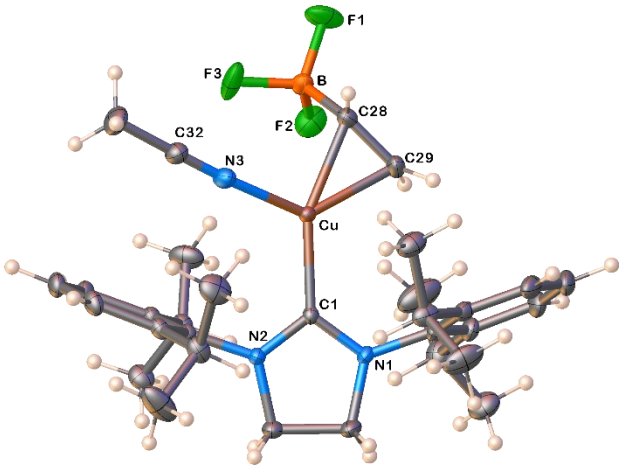

Figure 2. Molecular structure of (SIPr)Cu(MeCN)(CH_2=$CHBF_3$) (**4**). Selected bond distances (Å) and angles (°): C28-C29 1.3682(18), Cu-C1 1.9756(10), Cu-N3 1.9741(11), Cu-C28 2.1061(12), Cu-C29 2.0936(13), C28-B 1.6187(19), B-C28-Cu 109.52(8), C29-C28-B 122.87(12), C28-Cu-C29 38.03(5), C1-Cu-N3 112.78(4), Cu-N3-C32 174.50(12)

The copper(I) complex (SIPr)Cu(MeCN)(CH_2=$CHBF_3$) (**4**) has been characterized by X-ray crystallography (Figures 2). In contrast to the related silver analog (SIPr)Ag(CH_2=$CHBF_3$) (**3**), (SIPr)Cu(MeCN)(CH_2=$CHBF_3$) has an acetonitrile molecule coordinated to the metal ion, which is not lost under reduced pressure. The copper center is three-coordinate (which is a somewhat more common coordination number for copper over two coordinate systems)[14] and adopts a trigonal planar geometry. The carbons of [CH_2=$CHBF_3$]$^-$ group are marginally twisted (~10.4°) with respected to the N3-Cu-C1 plane. The Ag(CH_2=$CHBF_3$) moiety of the directly related (SIPr)Ag(CH_2=$CHBF_3$) shows positional disorder, and therefore is less useful for a detailed analysis. However, the NHC-silver complex (IPr*)Ag(CH_2=$CHBF_3$)[6] is known. A comparison of metal bound C=C bond distances in (IPr*)Ag(CH_2=$CHBF_3$)[6] and (SIPr)Cu(MeCN)(CH_2=$CHBF_3$) shows that it is longer in the latter (1.323(5) vs 1.3682(18) Å). In contrast to this silver complex, M-C(H_2) and M-C(BF_3) distances

are marginally different in **4** (e.g., 2.0936(13) and 2.1061(12) Å for the copper complex **4,** while 2.316(3) and 2.328(3) Å for (IPr*)Ag(CH_2=$CHBF_3$)) pointing to slightly asymmetric η^2-coordination. The Cu-C distances are shorter than Ag-C bond lengths which is expected based on the relatively smaller copper atom.

To rationalize the formation of (SIPr)Cu(MeCN)(CH_2=$CHBF_3$) instead of the acetonitrile free (SIPr)Cu(CH_2=$CHBF_3$), we calculated the free energy changes of reaction:

(SIPr)M(CH_2=$CHBF_3$) + MeCN → (SIPr)M(MeCN)(CH_2=$CHBF_3$) *eq. 1*

for M=Cu, Ag, and Au respectively, at the wB97XD/def2-TZVP level of DFT. Although the calculations showed that for all three metal ions, the three coordinate (SIPr)M(CH_2=$CHBF_3$) form is favored over (SIPr)M(MeCN)(CH_2=$CHBF_3$) (by 2.6, 5.8, and 6.1 kcal/mol, respectively), DFT correctly predicted that (SIPr)Cu(MeCN)(CH_2=$CHBF_3$) is easier to form than (SIPr)Ag(MeCN)(CH_2=$CHBF_3$).

Considering that the metal vinyltrifluoroborate complexes are rare and the NHC complexes afforded complexes **3** and **4** with different coordination numbers at the metal, we set out to uncover better examples that are more suitable for direct and detailed comparison of metal ion effects. The bis(3,5-dimethylpyrazolyl*)*methane (CH_2(3,5-$(CH_3)_2$Pz)$_2$) was chosen as the supporting ligand for this purpose.[15] The treatment of $(MeCN)_3$M(CH_2=$CHBF_3$) (M = Cu, Ag; generated in-situ from K(CH_2=$CHBF_3$) and $(MeCN)_4$Cu(BF_4) or $AgNO_3$ in acetonitrile) with CH_2(3,5-$(CH_3)_2$Pz)$_2$ gave [CH_2(3,5-$(CH_3)_2$Pz)$_2$]M(CH_2=$CHBF_3$) (**5** and **6**, Scheme 2) in over 90% yield. The [CH_2(3,5-$(CH_3)_2$Pz)$_2$]Cu(CH_2=$CHBF_3$) was obtained as a pale green solid while the silver analog is a white solid. Both are air stable and soluble in halogenated solvents like CH_2Cl_2 and $CHCl_3$ and insoluble in hexane and Et_2O. X-Ray quality

crystals of $[CH_2(3,5\text{-}(CH_3)_2Pz)_2]M(CH_2{=}CHBF_3)$ (M = Cu, Ag) were grown in vials open to air from a dichloromethane/hexane solution.

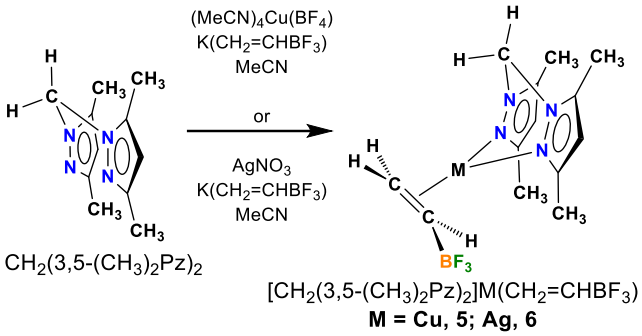

Scheme 2. Synthesis of $[CH_2(3,5\text{-}(CH_3)_2Pz)_2]Cu(CH_2{=}CHBF_3)$ (**5**) and $[CH_2(3,5\text{-}(CH_3)_2Pz)_2]Ag(CH_2{=}CHBF_3)$ (**6**)

The ^1H NMR spectra of $[CH_2(3,5\text{-}(CH_3)_2Pz)_2]M(CH_2{=}CHBF_3)$ display three sets of broad resonances for the protons of $CH_2{=}CHBF_3$ moiety. These signals of the copper complex $[CH_2(3,5\text{-}(CH_3)_2Pz)_2]Cu(CH_2{=}CHBF_3)$ (**5**) appear at a relatively upfield regions compared to those of the silver analog **6**, perhaps pointing to better backbonding between the metal and vinyltrifluoroborate in **5**.[16] The $^{13}C\{^1H\}$ NMR signal of the $\underline{C}H_2{=}CHBF_3$ was observed as a singlet at δ 87.3 and 102.2 ppm for $[CH_2(3,5\text{-}(CH_3)_2Pz)_2]Cu(CH_2{=}CHBF_3)$ and $[CH_2(3,5\text{-}(CH_3)_2Pz)_2]Ag(CH_2{=}CHBF_3)$, respectively. They show notable upfield shifts from the corresponding resonance for $K(CH_2{=}CHBF_3)$, which is detected at δ 121.6 ppm.[13] Those values represent about 33.4 and 19.4 ppm upfield shifts as a result of metal ion coordination. This trend of larger upfield shift of the olefinic ^{13}C signal upon copper ion coordination relative to that of silver is similar to those seen with previously reported ethylene complexes.[7b, 16-17]

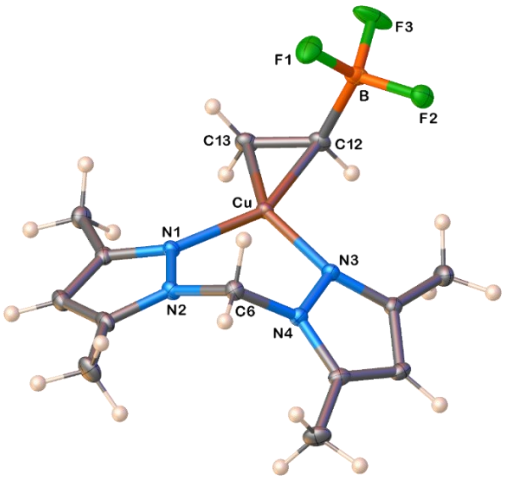

Figure 3. Molecular structure of $[CH_2(3,5\text{-}(CH_3)_2Pz)_2]Cu(CH_2{=}CHBF_3)$ (**5**).

Table 1. Selected bond distances (Å) and angles (°) of $LM(CH_2{=}CHBF_3)$; M = Cu, Ag, Au; L = $[CH_2(3,5\text{-}(CH_3)_2Pz)_2]$, and closest intra-molecular contacts (unless noted otherwise, i.e., if inter-molecular contacts are closer)

	Experiment (X-Ray)		Calculation (wB97xd/def2-tzvp)					
parameter	LCu ($CH_2{=}CHBF_3$)	LAg ($CH_2{=}CHBF_3$)	LCu ($CH_2{=}CHBF_3$)	LAg ($CH_2{=}CHBF_3$)	LAu ($CH_2{=}CHBF_3$)	Cu ($CH_2{=}CHBF_3$)	Ag ($CH_2{=}CHBF_3$)	Au ($CH_2{=}CHBF_3$)
C=C	1.371(3)	1.3674(16)	1.369	1.363	1.380	1.365	1.359	1.396
B-C	1.620(3)	1.6300(17)	1.646	1.651	1.661	1.655	1.654	1.668
M-C(H)$_2$	2.0279(17)	2.2562(11)	2.078	2.304	2.190	2.156	2.415	2.197
M-CH(BF_3)	2.0488(16)	2.3022(11)	2.053	2.280	2.212	2.070	2.326	2.208
M-N	1.9941(14)	2.2768(9)	2.043	2.325	2.871			
M-N	1.9910(14)	2.2454(9)	2.046	2.314	2.113			
C-M-C	39.31(7)	34.89(4)	38.7	34.6	36.5	37.6	33.3	37.0
C-C-B	122.27(17)	124.95(11)	124.3	125.4	124.9	125.0	124.8	124.6
M-C-B	110.16(11)	108.64(7)	96.1	96.6	106.3	85.1	86.9	98.8
N-M-N	96.86(6)	87.74(3)	92.1	83.0	73.7			
[b]N-M-C(H)$_2$	110.74(7)	115.61(4)	119.5	129.5	160.2			
[b]N-M-CH(BF_3)	113.43(7)	121.61(4)	109.4	108.0	88.6			
M-C-C-B	101.5	99.7	84.8	86.5	97.0	72.4	76.8	87.8
NMN/CMC	10.9	3.3	16.0	21.6	7.4			
F···H	*2.267*[a]	*2.384*[a]	2.202	2.248	2.225			
F···M	3.109	3.464	2.542	2.769	2.937	2.035	2.365	2.812
N-Au-C_{cent}	128.6	133.2	137.5	143.9	173.2			

[a]inter-molecular distances; [b]pyrazolyl nitrogen atom on the same side as the olefinic carbon; C_{cent} = C=C centroid

Crystals of $[CH_2(3,5\text{-}(CH_3)_2Pz)_2]Cu(CH_2{=}CHBF_3)$ (**5**) were investigated using X-ray crystallography at 100 K (Figure 3). Selected bond distances and angles are presented in Table 1. The bis(prazolyl)methane group adopts a half-chair conformation. The copper center has a trigonal planar geometry. The η^2-bound, $CH_2{=}CHBF_3$ moiety (CCuC plane) is slightly twisted (~10.9°) with respect to the NCuN plane. This distortion appears to be a steric effect caused by -BF_3 group on the olefinic carbon interacting with a methyl at the pyrazolyl ring 3-position. Note that the trigonal, in-plane conformation is the most stable geometry for ethylene-ML_2 complexes.[18] The C=C bond distance of $CH_2{=}CHBF_3$ moiety in **5** (1.371(3) Å) is essentially identical to that observed for **4** (1.3682(18) Å)**.** The Cu-C distances are slightly longer in the latter, which has a bulky NHC ligand support. Crystal packing diagram of $[CH_2(3,5\text{-}(CH_3)_2Pz)_2]Cu(CH_2{=}CHBF_3)$ shows intermolecular F•••H interactions between the fluorine atoms of BF_3 group and protons of methylene moiety as well as 5-methyl groups of the pyrazolyl rings (with closest F•••H at 2.27 Å).

The molecular structure of the silver(I) complex $[CH_2(3,5\text{-}(CH_3)_2Pz)_2]Ag(CH_2{=}CHBF_3)$ (**6**) is illustrated in Figure 4. Basic features are similar to those of the copper analog. As evident from the data presented in Table 1, the C=C bond distance of $CH_2{=}CHBF_3$ moiety is surprisingly similar between the two adducts. The Ag-C distances are however significantly longer than Cu-C separations of the copper adduct, which is expected due to the larger size of the silver atom. The metal-N distances also show a similar trend. The olefinic moiety of $CH_2{=}CHBF_3$ of **6** is essentially coplanar with the NAgN plane, likely as a result of larger separation of the two ligands on silver and therefore reduced steric interactions between the methyl and BF_3 groups. The metal-$C(H)_2$ distance is shorter than the M-$CH(BF_3)$ in both complexes indicating asymmetric η^2-coordination of the olefin group to the metal atom.

Molecules that show such deformation towards η^1-coordination (i.e., slippage from typical η^2 to pseudo η^1- coordination) are of significant current interest,[19] as they represent models for key bond making and olefin activation steps during metal-olefin chemistry.[9a] Investigation of crystal packing reveals that intermolecular F•••H interactions between the fluorine atoms of BF_3 group and protons of CH_2 moiety as well as 5-methyl groups of the pyrazolyl rings are also present in $[CH_2(3,5\text{-}(CH_3)_2Pz)_2]Ag(CH_2{=}CHBF_3)$ (with closest F•••H at 2.38 Å).

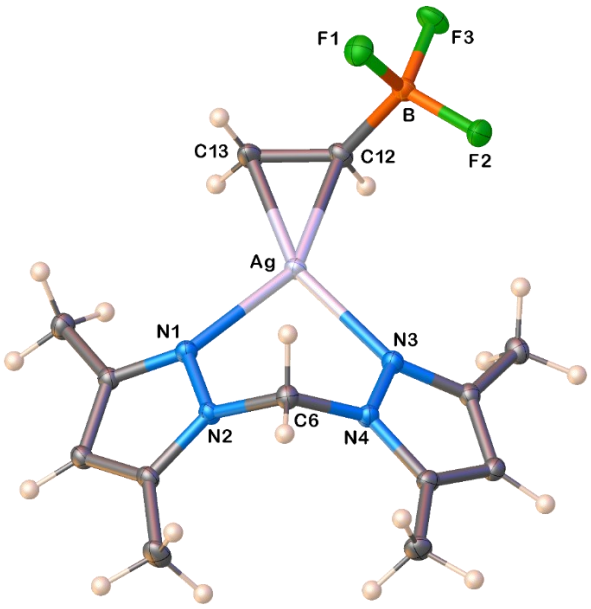

Figure 4. Molecular structure of $[CH_2(3,5\text{-}(CH_3)_2Pz)_2]Ag(CH_2{=}CHBF_3)$ (**6**).

The interactions between the metal center and the vinyl group were characterized using the density functional theory (DFT) calculations. To establish the level of theory used in the present study, we first compared the optimized geometries and calculated dissociation energies between ethylene and three coinage metal ions (Cu^+, Ag^+, and Au^+) between five widely used DFT functionals (B3LYP,[20] M06-2X,[21] wB97XD,[22] PBE0,[23] and BP86[23a, 24]). The results are presented in Tables S11 and S12.

Among the tested DFT methods, the wB97XD results agree best with reported experimental dissociation energies as well as with CCSD(T)/def2-QZVPP//CCSD/def2-TZVP calculation results. Reported benchmark work[25] also supports that wB97XD performs well for olefin metathesis reactions. Accordingly, all molecular geometry optimizations and interaction energies reported in this work are based on the wB97XD/def2-TZVP[26] level of theory.

The optimized structures of $[CH_2(3,5\text{-}(CH_3)_2Pz)_2]Cu(CH_2{=}CHBF_3)$ (**5**), $[CH_2(3,5\text{-}(CH_3)_2Pz)_2]Ag(CH_2{=}CHBF_3)$ (**6**), and the analogous complex involving Au were calculated using the level of theory mentioned above. Several key distances and angles are presented in Table 1 along with their corresponding values in the X-ray structures for **5** and **6**. Overall, the optimized structures agree well with the X-ray crystal structures. However, some notable differences are also observed, which we attribute to the change in the orientation of $CH_2{=}CHBF_3$ relative to $CH_2(3,5\text{-}(CH_3)_2Pz)_2$. For example, in crystal structures, the $-BF_3$ group forms an intermolecular H●●●F bonds with a nearby unit. Since this symmetry-related intermolecular interaction involving fluorides are not possible in the single molecule calculations, the $CH_2{=}CHBF_3$ moiety rotates slightly to form an intramolecular H●●●F contact with the $CH_2(3,5\text{-}(CH_3)_2Pz)_2$ fragment (Table 1). Furthermore, unlike the Cu and Ag analogs, the gold complex is notably distorted from ideal trigonal planar geometry as evident from the large N-Au-C angle of 160.2° (or N-Au-C_{cent} angle of 173.2°, C_{cent} = C=C centroid) and very different Au-N separations of 2.113 and 2.871 Å. We do not have experimental data of the gold complex thus far (synthesis of the gold adduct was attempted briefly by treating $[CH_2(3,5\text{-}(CH_3)_2Pz)_2]Ag(CH_2{=}CHBF_3)$ with AuCl but yielded only decomposed products) for a direct comparison.

To characterize the intrinsic interactions between the coinage metal ion and π-donor ligand, we calculated the structures and energies of metal-ethylene and metal-vinyltrifluoroborate complexes, and analyzed the nature of the metal-ligand interactions with the EDA (Energy Decomposition Analysis) partitioning scheme[27] in conjunction with the NOCV (Natural Orbitals for Chemical Valence) method.[28] The results of EDA are presented in Table 2. In a typical EDA partitioning scheme, the overall interaction between fragments can be decomposed into two terms, the frozen density component and the orbital interaction term:[27]

$$\Delta E_{int} = \Delta E_{frz} + \Delta E_{orb} \quad (1)$$

The frozen density term (i.e., ΔE_{frz}) can be further decomposed into a quasiclassical Coulomb electrostatic interaction and Pauli exchange repulsion.[27] Since the sum of the two terms corresponds to the interaction energy of the complex without any relaxation of molecular orbitals on each fragment, we do not to separate them in this study.

Table 2. Results of the EDA-NOCV calculations. The LM were treated as one fragment (all energies in kcal/mol), L = $[CH_2(3,5\text{-}(CH_3)_2Pz)_2]$, M = Cu, Ag, Au, L' = $C_2H_3BF_3$ moiety.

	ΔE(int)	ΔE(frz)	ΔE(orb)	σ donation	π backdonation	σ/E(orb)[a]	π/E(orb)[a]
M	$[M(C_2H_4)]^+$						
Cu	-53.15	-4.56	-48.60	-26.25	-10.54	54.01%	21.70%
Ag	-35.91	0.11	-36.02	-21.45	-6.19	59.55%	17.19%
Au	-67.62	13.31	-80.93	-46.58	-17.65	57.56%	21.81%
	$M(CH_2{=}CHBF_3)$						
Cu	-170.95	-107.46	-63.49	-23.48	-13.00	36.99%	20.47%
Ag	-143.06	-98.38	-44.69	-20.42	-6.13	45.70%	13.71%
Au	-172.58	-85.95	-86.63	-48.79	-14.97	56.31%	17.28%
	$LM(CH_2{=}CHBF_3)$						
Cu	-123.00	-65.57	-57.43	-18.46	-19.81	32.14%	34.49%
Ag	-110.75	-65.63	-45.12	-17.26	-10.19	38.26%	22.58%
Au	-139.49	-64.94	-74.55	-36.15	-17.11	48.49%	22.95%

[a]Percentage of the contribution of σ donation and π backdonation to ΔE(orb) term.

The orbital interaction term (i.e., ΔE_{orb}) is associated with the energy lowering due to the orbital relaxation after the formation of a complex and can be identified as covalent contribution to the chemical bond.[28] With the NOCV method, we can further decompose the orbital interaction term into pairwise orbital contributions of the interacting fragments, which can provide an important insight into the nature of the metal-ligand interactions. For example, in our recent study,[6] we have shown that for the system composed of a coinage metal ion and a π-donor ligand, the first two dominant terms in ΔE_{orb} can be viewed as the metal←ligand σ donation (i.e., the donation of electrons from the occupied π orbital of the olefin ligand to the vacant orbital of the metal ion) and metal→ligand π backdonation (from occupied d-orbital of the metal ion to the vacant π* orbital of the olefin ligand) of the standard DCD (Dewar-Chatt-Duncanson) model.[29] The remaining orbital interactions are from weak δ bonding and polarization of the fragments. Therefore, we only report the terms associated with the metal←olefin ligand σ donation and the metal→olefin ligand π backdonation in Table 2.

As shown in Table 2, the order of Au > Cu > Ag is well kept within the same olefin ligand (CH_2=CH_2 or [CH_2=$CHBF_3$]$^-$) with respect to the strengths of total interaction, orbital interaction, σ donation, or π backdonation for [M(CH_2=CH_2)]$^+$ and M(CH_2=$CHBF_3$) systems. This trend is also in good agreement with the previously reported work.[30] Since [CH_2=$CHBF_3$]$^-$ group is negatively charged, it is not surprising that the total interactions (ΔE_{int}) and the frozen density terms (ΔE_{frz}) of M(CH_2=$CHBF_3$) have increased significantly relative to the [M(CH_2=CH_2)]$^+$ system.

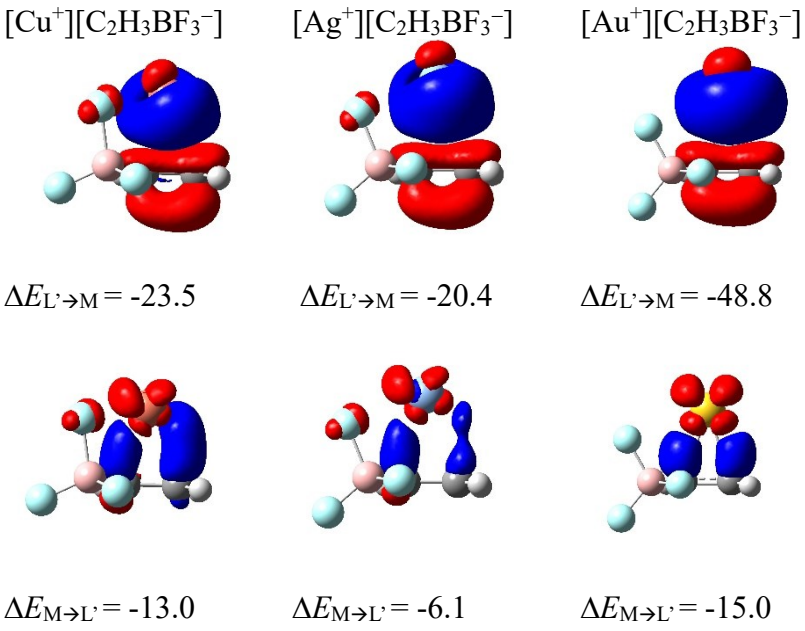

Figure 5. Plot of the deformation densities of the two most important pairwise orbital interactions associated with the orbital energies in the $[M^+][C_2H_3BF_3^-]$ complexes, with M = Cu, Ag, Au and L' = $C_2H_3BF_3$. Top panel shows the deformation densities due to the σ donation interactions with the NOCV pairwise orbital interaction energies, and the bottom panel the deformation densities due to the π backdonation with corresponding pairwise interaction energies. The energies are in unit of kcal/mol, and the direction of the charge flow is red → blue.

Our previous work on silver(I)[6] has shown that the Ag^+←olefin σ donation and Ag^+→olefin π backdonation exhibit a very similar strength between the $[Ag(CH_2{=}CH_2)]^+$ and $Ag(CH_2{=}CHBF_3)$ systems. The same trend is also observed for Cu and Au in the present calculations (Table 2). The shape of the deformation densities for the M←L' σ donation and M→L' π backdonation interactions, respectively, are illustrated in Figure 5 (L' = $C_2H_3BF_3$). For all three coinage metals (i.e., Cu, Ag, and Au), the M← olefin ligand σ donation and M→ olefin ligand π backdonation are different by less than 3 kcal/mol between $CH_2{=}CH_2$ and $CH_2{=}CHBF_3$; For the sum of

the two interactions, their difference between the two systems is less than 1.1 kcal/mol for each metal. In contrast, the total orbital interaction energy (ΔE_{orb}) increases by 5.7 kcal/mol for Au, 8.7 kcal/mol for Ag, and 14.9 kcal/mol for Cu between the two systems. This indicates that although each of the other orbital interactions contributes little to the total orbital interaction, their cumulative contribution increases from CH_2=CH_2 to CH_2=$CHBF_3$.

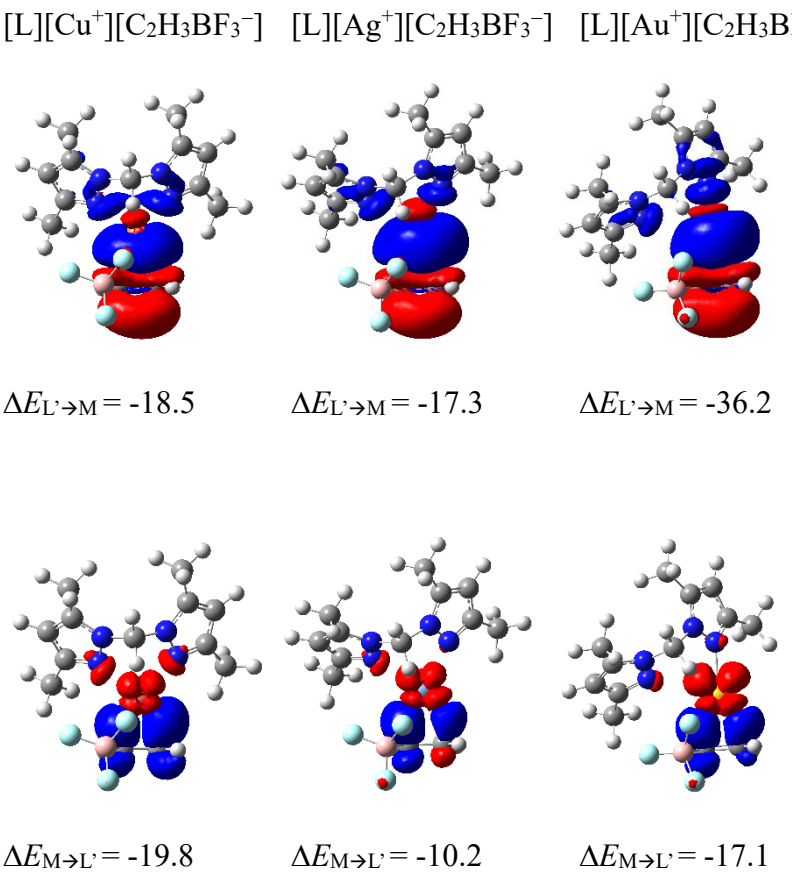

Figure 6. Plot of the deformation densities of the two most important pairwise orbital interactions that are associated with the orbital energies in the [L][M^+][$C_2H_3BF_3^-$] complexes, with L = CH_2(3,5-$(CH_3)_2$Pz)$_2$, L' = $C_2H_3BF_3$ and M = Cu, Ag, Au. Top panel shows the deformation densities due to the σ donation interactions with the NOCV pairwise orbital interaction energies, and the bottom panel shows the deformation densities due to the π backdonation with corresponding pairwise interaction energies. The energies are in unit of kcal/mol, and the direction of the charge flow is red → blue.

In Table 2, we also present the EDA-NOCV analysis data for [CH_2(3,5-$(CH_3)_2Pz)_2$]M(CH_2=$CHBF_3$) systems, and in Figure 6, the shape of the deformation densities for the M←L' σ donation and M→L' π backdonation interactions, respectively (M = Cu, Ag, Au; L' = $C_2H_3BF_3$). It emerges from the figure the substantial delocalization of the positive charge of M towards the CH_2(3,5-$(CH_3)_2Pz)_2$ ligand, which is not possible in the M(CH_2=$CHBF_3$) system. As a result, the electrostatic interaction with the CH_2=$CHBF_3$ (L') fragment is decreased substantially, which is evident from the decreased frozen density term (ΔE_{frz}) (Table 2). Interestingly, for this [CH_2(3,5-$(CH_3)_2Pz)_2$]M(CH_2=$CHBF_3$) complex, the magnitudes of the frozen density term are very close between the different metal ions. Thus, the order of the total interactions is solely determined by the order of the orbital interactions, i.e., Au > Cu > Ag. We note that this order in the orbital interaction terms is the same for the M(CH_2=CH_2) and M(CH_2=$CHBF_3$) systems, suggesting that this is an intrinsic property of the interaction between the C=C bond and the metal ions. This order is also reflected in the order of C=C double bond lengths of the CH_2=$CHBF_3$ fragment in each complex (Table 1). Namely, since both M←L' σ donation (removal of electron density from the C-C π orbital) and M→L' π backdonation (increase of electron density in the π* orbital) should lead to an elongation of the C=C double bond, stronger their interactions results in longer C=C bond. The C=C double bond length therefore can be viewed as a measurement of the strength of ΔE_{orb} between metal and π-donor ligand. As shown in Table 1, both experimental measurements and calculation results of the C=C double bond lengths are in good agreement with the order of the calculated orbital interactions.

Examining in more detail the σ donation and π backdonation terms, we find that while the order of σ donation and that of the total orbital interactions remain the same,

i.e., Au > Cu > Ag, the order of π backdonation flips between Cu and Au in the $[CH_2(3,5\text{-}(CH_3)_2Pz)_2]M(CH_2{=}CHBF_3)$ system. However, given the relatively small difference in their interaction energies (i.e., < 3 kcal/mol) and the difference in their (optimized) geometries (trigonal planar vs. approaching linear, Table 1), we believe this change in the π backdonation order is possible. In addition, the magnitude of the π backdonation is slightly larger than that of the σ donation in the metal-olefin fragment of the $[CH_2(3,5\text{-}(CH_3)_2Pz)_2]Cu(CH_2{=}CHBF_3)$ system, while the σ donation is consistently larger in all other systems. In fact, this is the first time that we observed a larger contribution of the π backdonation (albeit the difference is minor) to the total orbital interaction energy than that of the σ donation in these types of metal-olefin complexes, but it is not unusual in metal olefin complexes.[31]

Furthermore, the strength of the σ donation decreases going from the $M(CH_2{=}CHBF_3)$ complex to the $[CH_2(3,5\text{-}(CH_3)_2Pz)_2]M(CH_2{=}CHBF_3)$ complex, while the π backdonation follows the opposite trend. This is perhaps because the nitrogen donor $CH_2(3,5\text{-}(CH_3)_2Pz)_2$ ligand makes the metal sites less electrophilic relative to the supporting ligand free systems. Interestingly, this trend is different,[6] when different *N*-heterocyclic carbenes (NHCs) were used as the supporting ligand on Ag(I). It was found upon coordination of two different NHCs (i.e., 1,3-bis(2,6-diisopropylphenyl)imidazol-2-ylidene and 1,3-bis(2,6-diisopropylphenyl)imidazolin-2-ylidene), both σ donation and π backdonation interactions decreased. It remains interesting to further investigate the mechanism of how supporting ligand influences the interactions between the metal and the π-donor ligand.

We have also examined M-C bond distances of vinyltrifluoroborate complexes to see if they prefer η^2-symmetric or somewhat asymmetric bond formation to the metal site. As noted earlier, X-ray data (Table 1) show that $[CH_2(3,5\text{-}(CH_3)_2]M(CH_2{=}CHBF_3)$

complexes (M = Cu, Ag) feature shorter M-C(H)$_2$ distances (compared to M-CH(BF_3) distances), but steric factors and intermolecular H•••F contacts could have an effect of M-C distances. Computed structures of [CH_2(3,5-(CH_3)$_2$Pz)$_2$]M(CH_2=$CHBF_3$) and the supporting ligand free M(CH_2=$CHBF_3$) also show somewhat asymmetrically bound CH_2=$CHBF_3$ groups, but trend is opposite in which the M-CH(BF_3) is the shorter distance for each metal (Table 1, M = Cu, Ag). Unfortunately, BF_3 moieties of these molecules feature intramolecular H•••F and/or M•••F interactions, interfering with the M-C bond-distance analysis. Although it is tempting to use data from M(CH_2=$CHBF_3$) to indicate the preference for the η^2-(CH_2=$CHBF_3$) to bind Cu(I) and Ag(I) asymmetrically with a slightly shorter M-CH(BF_3) distances, considering the conflicting trends and inter- or intra-molecular contacts involving fluorine of BF_3 group, more data are useful before reaching a firm conclusion. It is noteworthy that a recent study reveals such interactions involving fluorines play an important role in silver phenyltrifluoroborate chemistry.[10b]

Finally, having synthesized ($MeCN)_3$Cu(CH_2=$CHBF_3$) using a copper(I) salt and K(CH_2=$CHBF_3$), we also explored the synthetic/catalytic potential of the pre-formed copper vinyltrifluoroborate, "Cu(CH_2=$CHBF_3$)". The 1,2-disubstituted cyclopropanes play a significant role as structural motifs in drug discovery.[32] Motivated by the work performed by Hryschuk and co-workers,[12] we attempted to use ($MeCN)_3$Cu(CH_2=$CHBF_3$) to access functionalized 1,2-disubstituted cyclopropane boronic derivatives. It was found that in acetone at 40 °C, preformed ($MeCN)_3$Cu(CH_2=$CHBF_3$) catalyzed (10 mol% loading) the reaction of ethyl diazoacetate with K(CH_2=$CHBF_3$) at 1:1 molar ratio affording the diastereomers of functionalized cyclopropyl trifluoroborate in 69% yield, which is comparable to yields reported earlier using a copper catalyst $CuPF_6$ with ethyl diazoacetate and

$K(CH_2{=}CHBF_3)$.[12]

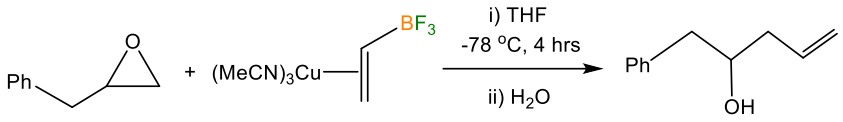

Scheme 3. Ring opening of 2-benzyloxirane with $(MeCN)_3Cu(CH_2{=}CHBF_3)$

Additionally, we also explored the utility of the pre-formed copper vinyltrifluoroborate in a ring opening reaction of an unhindered epoxide, 2-benzyloxirane, analogous to the lower order organocuprate work reported by Lipshutz *et al* using vinyllithium, $BF_3{\bullet}Et_2O$ and CuI in THF (Scheme 3).[11b] The authors reported that $BF_3{\bullet}Et_2O$ not only activates substrate but also modifies the organocuprate itself. We postulate that the identity of this lower order organocuprate in the presence of boron trifluoride could be similar to the pre-formed copper vinyltrifluoroborate "$Cu(CH_2{=}CHBF_3)$" described in this manuscript. A reaction of $(MeCN)_3Cu(CH_2{=}CHBF_3)$ with 2-benzyloxirane under reaction conditions similar to described by these authors[11b] indeed led to 1-phenylpent-4-en-2-ol in 63% yield, as confirmed by NMR spectroscopy. The vinyllithium, $BF_3{\bullet}Et_2O$ and CuI mixture in 1:1:1 molar ratio has reported to generate this product in 29% yield along with an additional by product, 1-iodo-3-phenyl-propanol. Although we had to increase reaction time to 4 hours for complete conversion, preformed $(MeCN)_3Cu(CH_2{=}CHBF_3)$ gave the ring open product more cleanly in greater yield. Thus, it is possible that "$Cu(CH_2{=}CHBF_3)$" species could play a role in copper-mediated transformation involving vinyllithium, $BF_3{\bullet}Et_2O$ and CuI in THF.

Summary and conclusions:

We have successfully isolated and completely characterized copper(I) and silver(I) complexes $[CH_2(3,5\text{-}(CH_3)_2Pz)_2]Cu(CH_2{=}CHBF_3)$, $(SIPr)Cu(MeCN)(CH_2{=}CHBF_3)$ and $[CH_2(3,5\text{-}(CH_3)_2Pz)_2]Ag(CH_2{=}CHBF_3)$ featuring a vinyltrifluoroborate. Spectroscopic data of $(MeCN)_3M(CH_2{=}CHBF_3)$ (M = Cu, Ag) are also presented. X-ray crystal structures show vinyltrifluoroborate moieties bonded somewhat asymmetrically to the metal site with relatively shorter M-$C(H)_2$ distances. However, DFT analysis of the M-C distances of $[CH_2(3,5\text{-}(CH_3)_2Pz)_2]M(CH_2{=}CHBF_3)$ and $M(CH_2{=}CHBF_3)$ predicts that M-$C(H)BF_3$ distances are shorter than M-$C(H)_2$ distances. These variations appear to be a result of inter- and/or intra-molecular contacts involving fluorine of BF_3 group. Total interactions (ΔE_{int}) and the frozen density terms (ΔE_{frz}) of $M(CH_2{=}CHBF_3)$ show significantly greater stabilization relative to the corresponding $[M(CH_2{=}CH_2)]^+$ systems (M = Cu, Ag, Au). The supporting ligand $CH_2(3,5\text{-}(CH_3)_2Pz)_2$ on $[CH_2(3,5\text{-}(CH_3)_2Pz)_2]M(CH_2{=}CHBF_3)$ systems leads to notable reduction in electrostatic interaction with the $CH_2{=}CHBF_3$ fragment relative to that in $M(CH_2{=}CHBF_3)$. The EDA-NOCV analysis of $[CH_2(3,5\text{-}(CH_3)_2Pz)_2]Cu(CH_2{=}CHBF_3)$ with $[CH_2(3,5\text{-}(CH_3)_2Pz)_2]Ag(CH_2{=}CHBF_3)$ shows that the copper center features a stronger σ– and π–interactions with $CH_2{=}CHBF_3$ fragment. The $(MeCN)_3Cu(CH_2{=}CHBF_3)$ serves as a catalyst for the carbene insertion to $K(CH_2{=}CHBF_3)$ leading to 1,2-disubstituted cyclopropyltrifluoroborates, and as an effective stoichiometric reagent to facilitate ring opening reactions of 2-benzyloxirane. We are presently exploring new transition metal chemistry of unsaturated organotrifluoroborate ligands.

Experimental section

All experiments were performed in open atmosphere unless otherwise specified. Solvents were procured from commercial sources and distilled from conventional drying agents prior to use. Glassware was oven dried at 150 ºC overnight. The NMR spectra were recorded at room temperature on a JEOL Eclipse 500 spectrometer (^{1}H, 500.16 MHz; ^{13}C, 125.77 MHz and ^{19}F, 470.62 MHz) and a JEOL Eclipse 300 spectrometer (^{11}B, 96.42 MHz). Proton and carbon chemical shifts are reported in ppm and are referenced using the residual proton and carbon signals of the deuterated solvent (^{1}H, $CDCl_3$, δ = 7.26 ppm; ^{13}C, $CDCl_3$, δ = 77.16 ppm). ^{19}F NMR chemical shifts were referenced relative to external $CFCl_3$. ^{11}B NMR was referenced to external BF_3•Et_2O. IR spectra were collected at room temperature on a Shimadzu IRPrestige-21 FTIR instrument containing an ATR attachment at 2 cm^{-1} resolution. Elemental analysis was performed at Intertek USA, Whitehouse, NJ. Deuterated solvents were purchased from Acros Organics and Cambridge Isotope Laboratories, respectively. $K(CH_2{=}CHBF_3)$,[13] $CH_2(3,5\text{-}(CH_3)_2Pz)_2$[33] and $(SIPr)CuNO_3$[34] were prepared according to literature procedure.

(SIPr)Cu(MeCN)(CH_2=CHBF_3): $(SIPr)CuNO_3$ (100 mg, 0.19 mmol) and $K(CH_2{=}CHBF_3)$ (28 mg, 0.21 mmol) in 7 mL of dichloromethane and 3 mL of acetonitrile were placed in a Schlenk tune and stirred overnight at room temperature. The resulting mixture was filtered through Celite and the solvent was removed under reduced pressure to give a white solid, $(SIPr)Cu(MeCN)(CH_2{=}CHBF_3)$. X-ray quality crystals were obtained from dichloromethane/hexane at room temperature. Yield: 90 %. ^{1}H NMR (in $CDCl_3$): δ (ppm) 7.43 (t, *J* = 8.0 Hz, 2H, CH_{Ar}), 7.26 (d, *J* = 8.0 Hz, 4H, CH_{Ar}), 5.06 (br m, 1H, CH_2CHBF_3), 4.66 (br d, *J* = 24.1 Hz, 1H, CH_2CHBF_3*)*, 4.36 (br d, 1H, CH_2CHBF_3), 4.07 (s, 4H, NCH_2), 3.02 (sept, *J* = 6.8 Hz, 4H, C*H*$(CH_3)_2$), 2.24

(s, 3H, CH_3CN), 1.33 (d, J = 6.9 Hz, 12 H, CH_3), 1.32 (d, J = 6.9 Hz, 12H, CH_3). $^{13}C\{^1H\}$ NMR (in $CDCl_3$): δ (ppm) 201.7 (*C*Cu), 146.7, 134.0, 130.1, 124.6, 118.1 (MeCN), 99.9 (CH_2=$CHBF_3$), 53.8 (N*C*H_2), 28.9 (*C*H(CH_3)$_2$), 25.1 (CH(*C*H_3)$_2$), 24.2 (CH(*C*H_3)$_2$), 2.4 (MeCN). ^{19}F NMR (in $CDCl_3$,): δ (ppm) -149.5 (br s, CH_2CHBF_3). ^{11}B NMR (in $CDCl_3$): δ (ppm) -1.16 (q, J = 7.2 Hz, CH_2CH*B*F_3) ppm. $C_{33}H_{58}BCuF_3N_3$ (628.19) Anal. calc.: C, 63.09%; H, 9.31%; N, 6.69%. Found: C, 63.28%; H, 9.48%; N, 6.42%.

(MeCN)$_3$Cu(CH_2=$CHBF_3$): $(MeCN)_4Cu(BF_4)$ (350 mg, 1.11 mmol) and K(CH_2=$CHBF_3$) (148 mg, 1.11 mmol) were taken in 7 mL of acetonitrile under nitrogen and the mixture was stirred overnight at room temperature. The mixture was filtered with celite. A small aliquot was withdrawn from the filtrate and analysed. Prolonged drying leads to sample decomposition. This product was used directly in the synthesis of [CH_2(3,5-(CH_3)$_2$Pz)$_2$]Cu(CH_2=$CHBF_3$) as noted below. ^1H NMR (in $CDCl_3$): δ (ppm) 5.27 (m, 1H, CH_2CHBF_3), 4.83 (dd, 1H, J = 2.9 Hz, J = 19.2 Hz CH_2CHBF_3), 4.63 (br d, 1H, J = 11.7 Hz, CH_2CHBF_3), 2.14 (s, 9H, MeCN). $^{13}C\{^1H\}$ NMR (in $CDCl_3$): δ (ppm) 117.6 (N*C*CH_3), 93.9 (*C*H_2CHBF_3), 2.6 (NC*C*H_3). ^{19}F NMR (in $CDCl_3$): δ (ppm) -142.4 (br s, CH_2CHBF_3).

[CH_2(3,5-(CH_3)$_2$Pz)$_2$]Cu(CH_2=$CHBF_3$): CH_2(3,5-(CH_3)$_2$Pz)$_2$ (212 mg, 1.11 mmol) dissolved in dichloromethane (7 mL) was added dropwise to the $(MeCN)_3Cu(CH_2=CHBF_3)$ obtained as noted above**,** and stirred overnight. The resulting mixture was then filtered and the solvent was removed under reduced pressure to give a slightly pale green solid, [CH_2(3,5-(CH_3)$_2$Pz)$_2$]Cu(CH_2=$CHBF_3$)**.** X-ray quality crystals were grown from dichloromethane/hexane at room temperature. Yield:

92%. ^{1}H NMR (in $CDCl_3$): δ (ppm) 6.08 (s, 2H, N(C*H*$_2$)N), 5.87 (s, 2H, CH_{pz}), 5.32 (m, 1H, CH_2CHBF_3), 4.83 (br d, 1H, *J* = 18.3 Hz, CH_2CHBF_3), 4.61 (br d, 1H, *J* = 12.6 Hz, CH_2CHBF_3), 2.35 (s, 6H, C*H*$_3$), 2.31 (s, 6H, C*H*$_3$). ^{13}C{^{1}H} NMR (in $CDCl_3$): δ (ppm) 151.7 (s, C(CH_3)), 141.6 (s, C(CH_3)), 107.0 (s, CH Pz), 87.3 (s, *C*H_2CHBF_3), 57.3 (s, NCH_2), 31.1, 13.8 (s, CH_3), 10.9 (s, CH_3) ppm. ^{19}F NMR (in $CDCl_3$): δ (ppm) -140.1 (br s, CH_2CHBF_3). ^{11}B NMR (in $CDCl_3$): δ(ppm) -0.91 (br s, CH_2CHBF_3). IR (cm^{-1}): 1600, 1558, 1467, 1420, 1390, 1284, 1044, 985, 982, 953, 856, 803. $C_{13}H_{19}N_4CuBF_3$ (362.67) Anal. calc.: C, 43.05%; H, 5.28%; N, 15.45%. Found: C, 43.37%; H, 5.59%; N,15.36%.

(MeCN)$_3$Ag(CH_2=CHBF_3)*:* A mixture of $AgNO_3$ (150 mg, 0.58 mmol) and K(CH_2=CHBF_3) (78 mg, 0.58 mmol) were taken in 7 mL of acetonitrile and allowed to stir overnight at room temperature. The mixture was then filtered through celite. A small aliquot was withdrawn from the filtrate and analysed. Prolonged drying leads to sample decomposition. This product was used directly in the synthesis of [CH_2(3,5-(CH_3)$_2$Pz)$_2$]Ag(CH_2=CHBF_3) as noted below. ^{1}H NMR (in $CDCl_3$): δ (ppm) 6.19 (br m, 1H, CH_2CHBF_3), 5.59 (dd, 1H, *J* = 4.9 Hz, *J* = 19.2 Hz CH_2CHBF_3), 5.42 (br d, 1H, *J* = 8.0 Hz, CH_2CHBF_3), 2.15 (s, 9H, MeCN). ^{13}C{^{1}H} NMR (in $CDCl_3$): δ (ppm) 118.4 (s, N*C*CH_3), 108.7 (s, *C*H_2CHBF_3), 2.3 (s, NC*C*H_3). ^{19}F NMR (in $CDCl_3$): δ (ppm) -142.2 (br s, CH_2CHBF_3).

[CH_2(3,5-(CH_3)$_2$Pz)$_2$]Ag(CH_2=CHBF_3)*:* CH_2(3,5-(CH_3)$_2$Pz)$_2$ (96 mg, 0.47 mmol) dissolved in dichloromethane (7 mL) was added dropwise to the (MeCN)$_3$Ag(CH_2=CHBF_3) obtained above, and stirred overnight. The resulting mixture was filtered and the solvent was removed under reduced pressure to give a

white solid, $[CH_2(3,5\text{-}(CH_3)_2Pz)_2]Ag(CH_2{=}CHBF_3)$. X-ray quality crystals were grown with dichloromethane/hexane at room temperature. Yield: 92%. ^{1}H NMR (in $CDCl_3$): δ (ppm) 6.15 (m, 1H, *J* = 3.2 Hz, CH_2CHBF_3), 6.03 (s, 2H, N(C*H*$_2$)N), 5.88 (s, 2H, CH_{pz}), 5.59 (dd, 1H, *J* = 4.7 Hz, *J* = 18.3 Hz, CH_2CHBF_3), 5.31 (m, 1H, CH_2CHBF_3), 2.41 (s, 6H, C*H*$_3$), 2.27 (s, 6H, C*H*$_3$) ppm. ^{13}C{^{1}H} NMR (in $CDCl_3$): δ (ppm) 151.5 (s, C(CH_3)), 141.2 (s, C(CH_3)), 107.0 (s, CH Pz), 102.2 (s, *C*H_2CHBF_3), 58.1 (s, CH_2), 14.1 (s, CH_3), 11.2 (s, CH_3). ^{19}F NMR (in $CDCl_3$): δ (ppm) -142.0 (s, CH_2CHBF_3). ^{11}B NMR (in $CDCl_3$): δ (ppm) –1.24 (br s, CH_2CHBF_3). IR (cm^{-1}): 3362, 2971, 2926, 1619, 1557, 1464, 1420, 1383, 1376, 1353,1286, 1269, 1077, 1085, 1069, 1033, 1021, 1014, 997, 953, 930, 906. $C_{13}H_{19}N_4CuBF_3$ (362.67) Anal. calc.: C, 38.36%; H, 4.71%; N, 13.77%. Found: C, 38.61%; H, 4.89%; N, 13.36%.

Synthesis of diasteromers of (ethoxycarbonyl)cyclopropyltrifluoroborates

Ethyl diazoacetate (0.54 mL, 1.5 mmol, 90% solution in dichloromethane) was added dropwise to a solution of $(MeCN)_3Cu(CH_2{=}CHBF_3)$ (0.15 mmol, 10 mol%) and $K(CH_2{=}CHBF_3)$ (200 mg, 1.5 mmol) in 5 mL of acetone over a period of two hours. After the addition was completed, the reaction mixture was stirred for another two hours at 40 ºC. After cooling, the mixture was reduced to half its original volume and poured into 20 mL of hexane. A clayish brown precipitate was formed. The solvent was decanted, and the precipitate was dissolved in 10 mL of ethanol by heating. After a few minutes of heating, a white solid precipitated out and was immediately filtered and collected to obtain the *trans*-isomer, potassium *trans*-2-(ethoxycarbonyl)cyclopropyltrifluoroborate. This product was identified by comparing NMR data to those reported in the literature.[12] Yield 52%. ^{1}H NMR (in DMSO-*d*$_6$): δ (ppm) 3.96 (q, *J* = 7.6 Hz, 2H,), 1.11 (m, 4H,), 0.63 (d, *J* = 9.5 Hz, 1H,),

0.47 (t, J = 7.2 Hz, 1H,), -0.11 (br. s, 1H). The filtrate was evaporated *in vacuo* to give the *cis*-product, potassium *cis*-2-(ethoxycarbonylcyclopropyl)trifluoroborate. This product was identified by comparing NMR to those reported in the literature.[12] Yield 17%. ^{1}H NMR (in DMSO-d_6): δ (ppm) 3.92 (q, 2H, J = 7.1 Hz,), 1.26 (s, 1H), 1.13 (m, 3H), 0.76 (s, 1H), 0.59 (m, 1H), -0.07 (br. s, 1H). The ratio of *trans/cis*-isomers in the crude reaction mixture, 84:16. This ratio of trans/cis-isomers was estimated using the ^{19}F NMR spectrum as there are distinct peaks for *trans- and cis*-isomers of the product[12] and also for K(CH_2=$CHBF_3$). ^{19}F NMR (in DMSO-d_6): δ (ppm) -141.6 (br m) potassium *trans*-2-(ethoxycarbonyl)cyclopropyl trifluoroborate, -135.2 (br m) potassium *cis*-2-(ethoxycarbonyl)cyclopropyl trifluoroborate, and -139.6 (br m), unreacted K(CH_2=$CHBF_3$).

Ring opening reaction of oxiranes using ($MeCN)_3Cu(CH_2$=$CHBF_3$)

Procedure was modified slightly from available literature.[11b] Briefly, ($MeCN)_3Cu(CH_2$=$CHBF_3$) (89.25 mg, 0.317 mmol) was added dropwise to a solution of allylbenzene oxide (42.53 mg, 0.317 mmol) in THF (4 mL) at -78 ^{o}C. The reaction was allowed to proceed at this temperature for 4 hours. The reaction was then quenched with 4 mL of a 10% NH_4OH/90% saturated NH_4Cl solution. The crude mixture was analyzed using ^{1}H NMR to check for presence of 1-phenylpent-4-en-2-ol.[11b] Percent yield was calculated from ^{1}H NMR, using an internal standard of dimethylformamide. Yield 63%. ^{1}H NMR (in $CDCl_3$): δ (ppm) 7.30 (m, 5H), 5.90 (dddd, 1H, J = 10.0, 5.1, 4.8, 2.4 Hz), 5.08 (m, 2H), 3.49 (m, 2H), 2.84 (dd, 1H, J = 15, 5 Hz), 2.53 (m, 2H).

X-ray Data Collection and Structure Determinations

A suitable crystal covered with a layer of hydrocarbon/Paratone-N oil was selected and mounted on a Cryo-loop, and immediately placed in the low temperature nitrogen stream. The X-ray intensity data were measured at 100(2) K on a Bruker D8 Quest with a Photon 100 CMOS detector equipped with an Oxford Cryosystems 700 series cooler, a graphite monochromator, and a Mo Kα fine-focus sealed tube (λ = 0.71073 Å). Intensity data were processed using the Bruker Apex program suite. Absorption corrections were applied by using SADABS.[35] Initial atomic positions were located by SHELXT,[36] and the structures of the compounds were refined by the least-squares method using SHELXL[37] within Olex2 GUI.[38] All the non-hydrogen atoms were refined anisotropically. The hydrogen atoms of CH_2CHBF_3 moiety were located in difference Fourier maps, included and refined freely with isotropic displacement parameters. Remaining hydrogen atoms were included in their calculated positions and refined as riding on the atoms to which they are joined. X-ray structural figures were generated using Olex2.[38] Compound (SIPr)Cu(MeCN)(CH_2=$CHBF_3$) crystallizes with two molecules of dichloromethane, one of which was disordered but modelled satisfactorily. CCDC 2063572-2063574 files contain the supplementary crystallographic data. These data can be obtained free of charge via http://www.ccdc.cam.ac.uk/conts/retrieving.html or from the Cambridge Crystallographic Data Centre (CCDC), 12 Union Road, Cambridge, CB2 1EZ, UK). Additional details are provided in supporting information section.

Crystal Data for (SIPr)Cu(MeCN)(CH_2=$CHBF_3$)•2(CH_2Cl_2): $C_{33}H_{48}BCl_4CuF_3N_3$ (M =759.89 g/mol): monoclinic, space group $P2_1/n$ (no. 14), a = 10.7461(4) Å, b = 22.3203(8) Å, c = 16.4600(6) Å, β = 106.1390(10)°, V = 3792.4(2) Å^3, Z = 4, T = 100.0 K, μ(MoKα) = 0.899 mm^{-1}, *Dcalc* = 1.331 g/cm^3, 61121 reflections measured

(5.586° ≤ 2Θ ≤ 66.284°), 14453 unique (R_{int} = 0.0229, R_{sigma} = 0.0207) which were used in all calculations. The final R_1 was 0.0386 (I > 2σ(I)) and wR_2 was 0.1082 (all data).

Crystal Data for $[CH_2(3,5\text{-}(CH_3)_2Pz)_2]Cu(CH_2{=}CHBF_3)$: $C_{13}H_{19}BCuF_3N_4$ (M =362.67 g/mol): monoclinic, space group C2/c (no. 15), a = 22.2814(7) Å, b = 7.8139(3) Å, c = 20.3486(10) Å, β = 122.0380(10)°, V = 3003.2(2) Å^3, Z = 8, T = 100.0 K, μ(MoKα) = 1.487 mm^{-1}, *Dcalc* = 1.604 g/cm^3, 23153 reflections measured (6.544° ≤ 2Θ ≤ 66.278°), 5707 unique (R_{int} = 0.0387, R_{sigma} = 0.0355) which were used in all calculations. The final R_1 was 0.0381 (I > 2σ(I)) and wR_2 was 0.0892 (all data).

Crystal Data for $[CH_2(3,5\text{-}(CH_3)_2Pz)_2]Ag(CH_2{=}CHBF_3)$: $C_{13}H_{19}AgBF_3N_4$ (M =407.00 g/mol): monoclinic, space group $P2_1/n$ (no. 14), a = 11.3966(6) Å, b = 12.1819(7) Å, c = 12.0151(7) Å, β = 114.8850(10)°, V = 1513.21(15) Å^3, Z = 4, T = 99.98 K, μ(MoKα) = 1.364 mm^{-1}, *Dcalc* = 1.787 g/cm^3, 30566 reflections measured (5.014° ≤ 2Θ ≤ 76.166°), 7962 unique (R_{int} = 0.0262, R_{sigma} = 0.0253) which were used in all calculations. The final R_1 was 0.0243 (I > 2σ(I)) and wR_2 was 0.0612 (all data).

Theoretical methods:

Optimization and frequency calculations were performed with the GAUSSIAN 09 software suites[39] at the High Performance Computing Center North (HPC2N), Umeå, Sweden. Optimized structures were obtained using wB97XD[22] functional and def2-TZVP[26] basis sets. Energy minima of all optimized molecular geometries were confirmed by the frequency analysis. The EDA-NOCV analysis were performed using method implemented in ORCA[40] software with wB97X-D3[41] functional and old-

ZORA-TZVPP basis set, and the relativistic effect was included by ZORA (zeroth-order regular approximation)[42] method.

Supporting information available:

Spectroscopic data and spectra, additional X-ray crystallographic and computational data.

Conflict of interest

The authors declare no conflict of interest.

Acknowledgments. This work was supported by National Science Foundation under Grant No. CHE-1954456 (to H.V.R.D.) and Robert A. Welch Foundation (Grant Y-1289). The computations were performed on resources provide by the Swedish National Infrastructure for Computing (SNIC) at the High-Performance Computing Center North (HPC2N).

References:

1. (a) S. Darses and J.-P. Genet, *Chem. Rev.*, 2008, **108**, 288-325; (b) G. A. Molander and N. Ellis, *Acc. Chem. Res.*, 2007, **40**, 275-286; (c) G. A. Molander, *J. Org. Chem.*, 2015, **80**, 7837-7848; (d) A. J. J. Lennox and G. C. Lloyd-Jones, *Angew. Chem., Int. Ed.*, 2012, **51**, 9385-9388.
2. S. Banjo, E. Nakasuji, T. Meguro, T. Sato and N. Chida, *Chem. - Eur. J.*, 2019, **25**, 7941-7947.
3. C. R. Groom, I. J. Bruno, M. P. Lightfoot and S. C. Ward, *Acta Crystallogr., Sect. B*, 2016, **72**, 171-179.
4. (a) A. S. Batsanov, D. Hérault, J. A. K. Howard, L. G. F. Patrick, M. R. Probert and A. Whiting, *Organometallics*, 2007, **26**, 2414-2419; (b) C. Bresner, S. Aldridge, I. A. Fallis, C. Jones and L. L. Ooi, *Angew. Chem., Int. Ed.*, 2005, **44**, 3606-3609; (c) J. W. Bats, M. Scheibitz and M. Wagner, *Acta Crystallogr., Sect. C Cryst. Struct. Commun.*, 2003, **59**, m355-m357; (d) T. D. Quach, R. A. Batey and A. J. Lough, *Acta Crystallogr., Sect. E*, 2001, **57**, m320-m321; (e) W. Erb, J.-P. Hurvois, T. Roisnel and V. Dorcet, *Organometallics*, 2018, **37**, 3780-3790.
5. T. V. Ashworth, M. J. Nolte, R. H. Reimann and E. Singleton, *J. Chem. Soc., Chem. Commun.*, 1977, 937-939.
6. G. Wang, L. Pecher, G. Frenking and H. V. R. Dias, *Eur. J. Inorg. Chem.*, 2018, 4142-4152.
7. (a) A. Das, Y. Hua, M. Yousufuddin, T. R. Cundari, J. Jeon and H. V. R. Dias, *Eur. J. Inorg. Chem.*, 2016, **2016**, 995-1001; (b) H. V. R. Dias and J. Wu, *Organometallics*, 2012, **31**, 1511-1517; (c) A. H. Elashkar, D. Parasar, A. Munoz-Castro, C. M. Doherty, M. G. Cowan and H. V. R. Dias, *ChemPlusChem*, 2021, **86**, 364-372; (d) M. Fianchini, C. F. Campana, B. Chilukuri, T. R. Cundari, V. Petricek and H. V. R. Dias, *Organometallics*, 2013, **32**, 3034-3041; (e) A. Noonikara-Poyil, S. G. Ridlen and H. V. R. Dias, *Inorg. Chem.*, 2020, **59**, 17860-17865; (f) D. Parasar, A. H. Elashkar, A. A. Yakovenko, N. B. Jayaratna, B. L. Edwards, S. G. Telfer, H. V. R. Dias and M. G. Cowan, *Angew. Chem., Int. Ed.*, 2020, **59**, 21001-21006; (g) S. G. Ridlen, N. V. Kulkarni and H. V. R. Dias, *Inorg. Chem.*, 2017, **56**, 7237-7246; (h) J. Wu, A. Noonikara-Poyil, A. Munoz-Castro and H. V. R. Dias, *Chem. Commun.*, 2021, **57**, 978-981; (i) H. V. R. Dias and J. Lovely Carl, *Chem. Rev.*, 2008, **108**, 3223-3238.

8. G. A. Molander and M. R. Rivero, *Org. Lett.*, 2002, **4**, 107-109.
9. (a) O. Eisenstein and R. Hoffmann, *J. Am. Chem. Soc.*, 1981, **103**, 4308-4320; (b) L. L. Wright, R. M. Wing and M. F. Rettig, *J. Am. Chem. Soc.*, 1982, **104**, 610-612; (c) N. D. Shapiro and F. D. Toste, *PNAS*, 2008, **105**, 2779-2782.
10. (a) C. A. Theulier, Y. Garcia-Rodeja, N. Saffon-Merceron, K. Miqueu, G. Bouhadir and D. Bourissou, *Chem. Commun.*, 2021, **57**, 347-350; (b) F. Bathie, A. W. E. Stewart, A. J. Canty and R. A. J. O'Hair, *Dalton Trans.*, 2021, **50**, 1496-1506; (c) M. L. Lepage, H.-T. Kuo, A. Roxin, S. Huh, Z. Zhang, R. Kandasamy, H. Merkens, J. O. Kumlin, A. Limoges, S. K. Zeisler, K.-S. Lin, F. Benard and D. M. Perrin, *ChemBioChem*, 2020, **21**, 943-947.
11. (a) G. Helmchen and G. Wegner, *Tetrahedron Lett.*, 1985, **26**, 6051-6054; (b) B. H. Lipshutz, E. L. Elsworth and T. J. Siahaan, *J. Am. Chem. Soc.*, 1989, **111**, 1351-1358; (c) Y. Yamamoto, Y. Chounan, S. Nishii, T. Ibuka and H. Kitahara, *J. Am. Chem. Soc.*, 1992, **114**, 7652-7660.
12. O. V. Hryschuk, Y. Yurov, A. V. Tymtsunik, V. O. Kovtunenko, I. V. Komarov and O. O. Grygorenko, *Adv. Synth. Catal.*, 2019, **361**, 5428-5439.
13. R. A. Oliveira, R. O. Silva, G. A. Molander and P. H. Menezes, *Magn. Reson. Chem.*, 2009, **47**, 873-878.
14. M. A. Carvajal, J. J. Novoa and S. Alvarez, *J. Am. Chem. Soc.*, 2004, **126**, 1465-1477.
15. C. Pettinari and R. Pettinari, *Coord. Chem. Rev.*, 2005, **249**, 663-691.
16. (a) P. O. Oguadinma and F. Schaper, *Organometallics*, 2009, **28**, 6721-6731; (b) H. V. R. Dias and J. Wu, *Eur. J. Inorg. Chem.*, 2008, 509-522.
17. K. Klimovica, K. Kirschbaum and O. Daugulis, *Organometallics*, 2016, **35**, 2938-2943.
18. T. A. Albright, R. Hoffmann, J. C. Thibeault and D. L. Thorn, *J. Am. Chem. Soc.*, 1979, **101**, 3801-3812.
19. N. Phillips, R. Kong, A. White and M. R. Crimmin, *Angew. Chem., Int. Ed.*, **n/a**.
20. (a) S. H. Vosko, L. Wilk and M. Nusair, *Can. J. Phys.*, 1980, **58**, 1200-1211; (b) C. Lee, W. Yang and R. G. Parr, *Phys. Rev. B Condens. Matter*, 1988, **37**, 785-789; (c) A. D. Becke, *J. Chem. Phys.*, 1993, **98**, 5648-5652; (d) P. J. Stephens, F. J. Devlin, C. F. Chabalowski and M. J. Frisch, *J. Phys. Chem.*, 1994, **98**, 11623-11627.
21. Y. Zhao and D. G. Truhlar, *Theor. Chem. Acc.*, 2008, **120**, 215-241.

22. J.-D. Chai and M. Head-Gordon, *Phys. Chem. Chem. Phys.*, 2008, **10**, 6615-6620.
23. (a) J. P. Perdew, K. Burke and M. Ernzerhof, *Phys. Rev. Lett.*, 1996, **77**, 3865-3868; (b) J. P. Perdew, K. Burke and M. Ernzerhof, *Phys. Rev. Lett.*, 1997, **78**, 1396; (c) C. Adamo and V. Barone, *J. Chem. Phys.*, 1999, **110**, 6158-6170.
24. A. D. Becke, *Phys. Rev. A Gen. Phys.*, 1988, **38**, 3098-3100.
25. Y. Minenkov, A. Singstad, G. Occhipinti and V. R. Jensen, *Dalton Trans.*, 2012, **41**, 5526-5541.
26. (a) F. Weigend and R. Ahlrichs, *Phys. Chem. Chem. Phys.*, 2005, **7**, 3297-3305; (b) F. Weigend, *Phys. Chem. Chem. Phys.*, 2006, **8**, 1057-1065.
27. (a) K. Morokuma, *J. Chem. Phys.*, 1971, **55**, 1236-1244; (b) T. Ziegler and A. Rauk, *Theor. Chim. Acta*, 1977, **46**, 1-10.
28. (a) M. Mitoraj and A. Michalak, *J. Mol. Model.*, 2007, **13**, 347-355; (b) M. P. Mitoraj, A. Michalak and T. Ziegler, *J. Chem. Theory Comput.*, 2009, **5**, 962-975; (c) L. Zhao, M. von Hopffgarten, D. M. Andrada and G. Frenking, *WIREs Computational Molecular Science*, 2018, **8**, e1345.
29. (a) J. Chatt and L. A. Duncanson, *J. Chem. Soc.*, 1953, 2939-2947; (b) J. Chatt, L. A. Duncanson and L. M. Venanzi, *J. Chem. Soc.*, 1955, 4456-4460.
30. (a) R. H. Hertwig, W. Koch, D. Schroeder, H. Schwarz, J. Hrusak and P. Schwerdtfeger, *J. Phys. Chem.*, 1996, **100**, 12253-12260; (b) C. K. Kim, K. A. Lee, C. K. Kim, B.-S. Lee and H. W. Lee, *Chem. Phys. Lett.*, 2004, **391**, 321-324.
31. M. S. Nechaev, V. M. Rayon and G. Frenking, *J. Phys. Chem. A*, 2004, **108**, 3134-3142.
32. C. Ebner and E. M. Carreira, *Chem. Rev.*, 2017, **117**, 11651-11679.
33. C. T. Burns and R. F. Jordan, *Organometallics*, 2007, **26**, 6726-6736.
34. T. T. Ponduru, G. Wang, S. Manoj, S. Pan, L. Zhao, G. Frenking and H. V. R. Dias, *Dalton Trans.*, 2020, **49**, 8566-8581.
35. L. Krause, R. Herbst-Irmer, G. M. Sheldrick and D. Stalke, *J. Appl. Crystallogr.*, 2015, **48**, 3-10.
36. G. Sheldrick, *Acta Crystallogr. Sect. A: Found. Adv.*, 2015, **71**, 3-8.
37. G. Sheldrick, *Acta Crystallogr. Sect. C: Struct. Chem.*, 2015, **71**, 3-8.
38. O. V. Dolomanov, L. J. Bourhis, R. J. Gildea, J. A. K. Howard and H. Puschmann, *J. Appl. Crystallogr.*, 2009, **42**, 339-341.

39. Gaussian 09, Revision E.01, M. J. Frisch, G. W. Trucks, H. B. Schlegel, G. E. Scuseria, M. A. Robb, J. R. Cheeseman, G. Scalmani, V. Barone, B. Mennucci, G. A. Petersson, H. Nakatsuji, M. Caricato, X. Li, H. P. Hratchian, A. F. Izmaylov, J. Bloino, G. Zheng, J. L. Sonnenberg, M. Hada, M. Ehara, K. Toyota, R. Fukuda, J. Hasegawa, M. Ishida, T. Nakajima, Y. Honda, O. Kitao, H. Nakai, T. Vreven, J. A. Montgomery, Jr., J. E. Peralta, F. Ogliaro, M. Bearpark, J. J. Heyd, E. Brothers, K. N. Kudin, V. N. Staroverov, R. Kobayashi, J. Normand, K. Raghavachari, A. Rendell, J. C. Burant, S. S. Iyengar, J. Tomasi, M. Cossi, N. Rega, J. M. Millam, M. Klene, J. E. Knox, J. B. Cross, V. Bakken, C. Adamo, J. Jaramillo, R. Gomperts, R. E. Stratmann, O. Yazyev, A. J. Austin, R. Cammi, C. Pomelli, J. W. Ochterski, R. L. Martin, K. Morokuma, V. G. Zakrzewski, G. A. Voth, P. Salvador, J. J. Dannenberg, S. Dapprich, A. D. Daniels, Ö. Farkas, J. B. Foresman, J. V. Ortiz, J. Cioslowski, and D. J. Fox, Gaussian, Inc., Wallingford CT, 2009.

40. (a) F. Neese, *WIREs Computational Molecular Science*, 2012, **2**, 73-78; (b) F. Neese, *WIREs Computational Molecular Science*, 2018, **8**, e1327.

41. Y.-S. Lin, G.-D. Li, S.-P. Mao and J.-D. Chai, *J. Chem. Theory Comput.*, 2013, **9**, 263-272.

42. (a) C. Chang, M. Pelissier and P. Durand, *Phys. Scr.*, 1986, **34**, 394-404; (b) E. van Lenthe, E. J. Baerends and J. G. Snijders, *J. Chem. Phys.*, 1994, **101**, 9783-9792.